Gravitational torque-driven black hole growth and feedback in cosmological simulations

Monthly Notices of the ROYAL ASTRONOMICAL SOCIETY

MNRAS **464,** 2840–2853 (2017) doi:10.1093/mnras/stw2565
Advance Access publication 2016 October 8

Gravitational torque-driven black hole growth and feedback in cosmological simulations

Daniel Anglés-Alcázar,[1]★ Romeel Davé,[2,3,4] Claude-André Faucher-Giguère,[1] Feryal Özel[5] and Philip F. Hopkins[6]

[1]*Center for Interdisciplinary Exploration and Research in Astrophysics (CIERA) and Department of Physics and Astronomy, Northwestern University, 2145 Sheridan Road, Evanston, IL 60208, USA*
[2]*University of the Western Cape, Bellville, Cape Town 7535, South Africa*
[3]*South African Astronomical Observatories, Observatory, Cape Town 7925, South Africa*
[4]*African Institute for Mathematical Sciences, Muizenberg, Cape Town 7945, South Africa*
[5]*Astronomy Department, University of Arizona, Tucson, AZ 85721, USA*
[6]*TAPIR, Mailcode 350-17, California Institute of Technology, Pasadena, CA 91125, USA*

Accepted 2016 October 5. Received 2016 August 24; in original form 2016 March 20; Editorial Decision 2016 October 3

ABSTRACT

We investigate black hole–host galaxy scaling relations in cosmological simulations with a self-consistent black hole growth and feedback model. Our sub-grid accretion model captures the key scalings governing angular momentum transport by gravitational torques from galactic scales down to parsec scales, while our kinetic feedback implementation enables the injection of outflows with properties chosen to match observed nuclear outflows (star formation-driven winds are not included to isolate the effects of black hole feedback). We show that 'quasar mode' feedback can have a large impact on the thermal properties of the intergalactic medium and the growth of galaxies and massive black holes for kinetic feedback efficiencies as low as 0.1 per cent relative to the bolometric luminosity. None the less, our simulations indicate that the black hole–host scaling relations are only weakly dependent on the effects of black hole feedback on galactic scales, since black hole feedback suppresses the growth of galaxies and massive black holes by a similar amount. In contrast, the rate at which gravitational torques feed the central black hole relative to the host galaxy star formation rate governs the slope and normalization of the black hole–host correlations. Our results suggest that a common gas supply regulated by gravitational torques is the primary driver of the observed co-evolution of black holes and galaxies.

Key words: galaxies: active – galaxies: evolution – galaxies: formation – intergalactic medium – quasars: supermassive black holes – cosmology: theory.

1 INTRODUCTION

The energy released by accretion on to supermassive black holes may have a profound effect on the evolution of galaxies (Silk & Rees 1998; Somerville et al. 2008; Cattaneo et al. 2009). Indeed, contemporary models of galaxy formation appear to require feedback from active galactic nuclei (AGN) to suppress star formation in galaxies at high masses (Somerville & Davé 2015). Recent years have seen increasing observational evidence for AGN feedback, from radio-emitting jets powered by slowly accreting black holes to powerful winds driven by quasars (Fabian 2012; Heckman & Best 2014). While the overall effect is still unclear, the energy and momentum inferred from observed fast nuclear outflows (e.g. Tombesi et al. 2013; Nardini et al. 2015) and galaxy-scale winds (e.g. Feruglio et al. 2010; Rupke & Veilleux 2011; Sturm et al. 2011; Greene, Zakamska & Smith 2012; Maiolino et al. 2012; Liu et al. 2013; Cicone et al. 2014; Harrison et al. 2014) suggest that AGN feedback may have a significant impact on the evolution of massive black holes as well, particularly during phases of rapid growth where most black hole mass is believed to assemble (Soltan 1982; Yu & Tremaine 2002).

The observed correlations between the mass of central supermassive black holes and various stellar properties of their host galaxies (e.g. Häring & Rix 2004; Hopkins et al. 2007b; Gültekin et al. 2009; Graham & Scott 2013; McConnell & Ma 2013; Woo et al. 2013; van den Bosch 2016) are often interpreted as indirect evidence for the effects of feedback from black hole accretion on galactic scales.

★ E-mail: anglesd@northwestern.edu

Analytic models show that the black hole–galaxy scaling relations can be explained under the assumption that black holes regulate their own growth by the efficient coupling of feedback at galactic scales (Silk & Rees 1998; King 2003; Murray, Quataert & Thompson 2005; King & Pounds 2015). In these models, black holes grow to a critical mass at which feedback is able to expel the remaining gas in the galaxy, inhibiting further accretion as well as star formation in the host galaxy. This scenario has been extensively explored in numerical hydrodynamic simulations over the last decade, where 'sub-grid' models are introduced in order to incorporate black hole growth as well as the effects of feedback on galactic scales (e.g. Di Matteo, Springel & Hernquist 2005; Hopkins et al. 2005, 2006, 2007a; Springel, Di Matteo & Hernquist 2005; Sijacki et al. 2007, 2015; Booth & Schaye 2009; Filloux et al. 2010; Choi et al. 2012; Debuhr, Quataert & Ma 2012; Dubois et al. 2012; Rosas-Guevara et al. 2015; Steinborn et al. 2015). The success of these models in explaining many observables of galaxies and quasars has contributed to establishing a paradigm in which the observed connection between black holes and galaxies is driven by feedback from the black hole itself.

While feedback self-regulation represents an interesting possibility, the detailed physics and overall efficiency with which black hole-driven outflows interact with the inflowing gas feeding the accretion disc remain poorly understood. Regardless of the effects of feedback, the rate at which gravitational torques transport angular momentum at galactic scales may be the limiting factor for fuelling AGN (Hernquist 1989; Shlosman, Frank & Begelman 1989; Shlosman, Begelman & Frank 1990; Jogee 2006; Escala 2007; Hopkins & Quataert 2010; Cen 2015). Owing to its simplicity, most black hole accretion prescriptions used in hydrodynamic simulations of galaxy formation are based on the spherical Bondi parametrization (Bondi & Hoyle 1944; Bondi 1952). In the Bondi parametrization, the angular momentum of the inflowing gas is explicitly neglected. Hopkins & Quataert (2010) addressed the problem of AGN fuelling by performing multiple nested galaxy-scale simulations of progressively higher resolution. These simulations showed that non-axisymmetric perturbations to the stellar potential drive gas into shocks that dissipate energy and angular momentum, dominating the net torque on the gas component and driving gas inflows down to sub-parsec scales. Hopkins & Quataert (2011) derived an analytic accretion rate estimator that captures the key scalings found in the numerical simulations, while showing that the spherical Bondi parametrization systematically fails to reproduce the gas inflow rates. In very gas rich systems, efficient local fragmentation may provide additional mechanisms for angular momentum transport, including the scattering of dense gas clumps and gravitational instability-driven turbulence (Levine et al. 2008; Bournaud et al. 2011; Hopkins et al. 2016).

It is worth noting that the adoption of Bondi accretion in simulations automatically implies the need for self-regulation by feedback processes in order to reproduce the observed black hole–galaxy scaling relations. Indeed, any model in which the accretion rate depends on black hole mass as $\dot{M}_{\rm BH} \propto M_{\rm BH}^{p}$, with $p > 1$ as in Bondi ($p = 2$), yields divergent evolution of black hole mass relative to changes in the initial conditions unless additional feedback mechanisms ensure strong self-regulation (Anglés-Alcázar et al. 2015). The amount of feedback injected in the simulation relative to the accretion rate is generally chosen such that strong self-regulation occurs and yields the scaling relations (Di Matteo et al. 2005). It is thus critical to break the degeneracy between fuelling and feedback and evaluate their relative roles in driving the observed black hole–galaxy scaling relations.

Recently, Anglés-Alcázar, Özel & Davé (2013) and Anglés-Alcázar et al. (2015) proposed an alternative scenario to explain the black hole–galaxy scaling relations motivated by a careful examination of the implications of the black hole accretion parametrization. Post-processing cosmological simulations without AGN feedback, Anglés-Alcázar et al. (2013, 2015) showed that self-regulation by feedback processes may not be required when the physics of gravitational torques is appropriately captured at a sub-grid level. Instead, the rate at which gravitational torques drive gas inflows down to sub-parsec scales relative to the host galaxy star formation rate (SFR) modulates the long-term co-evolution of massive black holes and galaxies. In this torque-limited growth scenario, black holes and galaxies evolve on average towards the observed scaling relations, regardless of the initial conditions, and with no need for mass averaging through mergers (Peng 2007; Hirschmann et al. 2010; Jahnke & Macciò 2011) or additional self-regulation processes. While showing that there is no need to regulate black hole growth in a non-linear feedback loop, Anglés-Alcázar et al. (2013, 2015) did not address explicitly the role of AGN feedback in the black hole–galaxy connection.

Here, we perform cosmological hydrodynamic simulations that follow, for the first time, the evolution of massive black holes and galaxies using a new implementation of AGN feedback self-consistently coupled to black hole accretion driven by gravitational torques. Cosmological simulations will rely heavily on sub-grid models of black hole growth and feedback for the foreseeable future, emphasizing the importance of developing and testing models motivated by higher resolution calculations. In this work, we do not attempt to build a comprehensive galaxy formation model, as would be needed to make detailed comparisons to observations. Our main goal is rather to investigate the relative roles played by accretion and galaxy-scale AGN feedback in driving the overall connection between massive black holes and galaxies when adopting a physically motivated accretion model based on gravitational torques. We thus deliberately limit the complexity of galaxy formation physics included in our simulations and perform numerical experiments with various combinations of black hole model parameters.

We begin by summarizing the properties of our simulations in Section 2, including a description of our new implementation of black hole-driven outflows coupled to gravitational torque-driven accretion. We present the $M_{\rm BH}$–M_{*} relation predicted by our fiducial feedback simulation in Section 3, where we analyse its dependence on various model parameters and the similarities with the post-processing calculations of Anglés-Alcázar et al. (2013, 2015) neglecting black hole feedback. We illustrate the overall effects of AGN feedback in our simulations in Section 4, where we show the impact of kinetic outflows on the thermal properties of the intergalactic medium and the global growth of galaxies and massive black holes. We discuss the implications of our findings in Section 5 and present our conclusions in Section 6. Different aspects of the numerical robustness of our simulations are discussed in Appendix A.

2 SIMULATIONS

Our main simulations use the *N*-body + hydrodynamics simulation code GIZMO[1] (Hopkins 2015) in 'P-SPH' mode, a pressure–entropy formulation of smoothed particle hydrodynamics (SPH) that minimizes the errors of previous SPH formulations regarding

[1] www.tapir.caltech.edu/phopkins/Site/GIZMO.html

Table 1. Parameters of simulations. (1) Name: simulation designation. (2) $m_{\rm b}$: initial baryonic particle mass ($M_\odot\,h^{-1}$). (3) $\epsilon_{\rm b}$: minimum baryonic force softening length (h^{-1} kpc). (4) $M_{\rm seed}$: physical mass of black hole seeds ($M_\odot\,h^{-1}$). (5) $\epsilon_{\rm T}$: normalization of $\dot{M}_{\rm Torque}$. (6) $v_{\rm out}$: assumed velocity of AGN-feedback-driven outflows (km s^{-1}). (7) $p_{\rm b}$: total momentum flux of outflows in units of $L_{\rm bol}/c$. (8) $z_{\rm end}$: final simulation redshift. (9) $\dot{M}_{\rm out}/\dot{M}_{\rm BH}$: mass outflow rate relative to black hole accretion rate (determined by $v_{\rm out}$ and $p_{\rm b}$). (10) $\epsilon_{\rm k}$: kinetic feedback efficiency, defined as $\epsilon_{\rm k} \equiv \frac{1}{2}\dot{M}_{\rm out}v_{\rm out}^2 / L_{\rm bol}$ (determined by $v_{\rm out}$ and $p_{\rm b}$).

Name	$m_{\rm b}$	$\epsilon_{\rm b}$	$M_{\rm seed}$	$\epsilon_{\rm T}$	$v_{\rm out}$	$p_{\rm b}$	$z_{\rm end}$	Notes	$\dot{M}_{\rm out}/\dot{M}_{\rm BH}$	$\epsilon_{\rm k}$
n256-fid	6.4e6	0.16	10^5	0.5	10^3	1	0	Fiducial simulation	30	1.6e-3
n256s6	6.4e6	0.16	10^6	0.5	10^3	1	0	Overmassive seed	30	1.6e-3
n256s4	6.4e6	0.16	10^4	0.5	10^3	1	0	Undermassive seed	30	1.6e-3
n256eH	6.4e6	0.16	10^5	5	10^3	1	0	High normalization	30	1.6e-3
n256eL	6.4e6	0.16	10^5	0.05	10^3	1	0	Low normalization	30	1.6e-3
n256v4	6.4e6	0.16	10^5	0.5	10^4	1	0	High-velocity outflows	3	1.6e-2
n256p20	6.4e6	0.16	10^5	0.5	10^3	20	0	Large momentum boost	600	3.3e-2
n256-nf	6.4e6	0.16	10^5	0.5	0	0	0	No feedback	0	0
n256-mfm	6.4e6	0.16	10^5	0.5	10^3	1	0	Meshless hydrodynamics	30	1.6e-3
n512	8.0e5	0.08	10^5	0.5	10^3	1	2	High resolution	30	1.6e-3

fluid mixing instabilities (Hopkins 2013; Saitoh & Makino 2013). Gravitational forces are computed using a modified version of the tree-particle-mesh algorithm of the GADGET-2 code (Springel 2005), including adaptive gravitational softenings following Price & Monaghan (2007). We use the Durier & Dalla Vecchia (2012) time-step limiter to handle strong feedback events. With this limiter, particles are not allowed to have a time step >4 times larger than that of any active particle neighbour.

We include radiative cooling from primordial gas (Katz, Weinberg & Hernquist 1996), metal-line cooling (Wiersma, Schaye & Smith 2009), and photoionization heating from an optically thin UV background (Faucher-Giguère et al. 2009). Star formation is modelled following the sub-grid prescription of Springel & Hernquist (2003): gas particles with density $n_{\rm H} \gtrsim 0.13$ cm^{-3} are treated as a multi-phase fluid with cold clouds embedded in a hot medium (McKee & Ostriker 1977), which gives them an 'effective pressure' larger than the thermal pressure, based on sub-grid supernova heating. Gas particles are converted into star particles with a probability based on a Schmidt (1959) law, such that the resulting SFRs are in agreement with the observed Kennicutt (1998) relation.

We intentionally limit the complexity of stellar feedback physics included in our simulations to isolate the implications of the black hole parametrization. In particular, we do not include star formation-driven winds, which many previous studies showed are necessary to reproduce the properties of observed galaxies (e.g. Davé, Oppenheimer & Finlator 2011a; Davé, Finlator & Oppenheimer 2011b; Anglés-Alcázar et al. 2014). Our simulations show that the black hole–host scaling relations can robustly emerge from a gravitational torque-driven accretion model, independent of whether other processes such as stellar feedback act to reproduce the details of observed galaxy populations. This is in agreement with post-processing calculations of simulations with and without star formation-driven winds (Anglés-Alcázar et al. 2015). We will address the interaction of black holes with star formation-driven outflows in future work.

We adopt a 'standard' flat Λ cold dark matter cosmology with parameters $\Omega_\Lambda = 0.69$, $\Omega_{\rm M} = 0.31$, $\Omega_{\rm b} = 0.05$, $h = 0.68$, $\sigma_8 = 0.82$, and $n = 0.97$, consistent with Planck Collaboration XIII (2016). Our main simulation runs evolve a $[20\,h^{-1}\,{\rm Mpc}]^3$ comoving volume down to $z = 0$ employing 256^3 gas and 256^3 dark matter particles with masses $m_{\rm b} = 6.4 \times 10^6\,{\rm M}_\odot\,h^{-1}$ and $m_{\rm DM} = 3.4 \times 10^7\,{\rm M}_\odot\,h^{-1}$, respectively. Cosmological initial conditions were generated using MUSIC (Hahn & Abel 2011). The minimum comoving softening length is set to 2 per cent of the mean interparticle distance for dark matter particles, $\epsilon_{\rm DM} = 1.6\,h^{-1}$ kpc, while it is allowed to decrease down to $\epsilon_{\rm b} = 0.16\,h^{-1}$ kpc for baryonic particles (gas, stars, and black holes). The minimum SPH smoothing lengths are comparable to or smaller than the minimum softening length $\epsilon_{\rm b}$. We present a resolution convergence test in Appendix A1. The black hole accretion and feedback models used here are appropriate for large box simulations: our mass and force resolution are comparable to, e.g., the Illustris (Vogelsberger et al. 2014) and EAGLE (Schaye et al. 2015) simulations.

All runs use the same basic simulation parameters with the exception of quantities specific to black hole accretion and feedback, which are varied as described below. Moreover, we evaluate the robustness of our results with respect to the hydrodynamics solver in Appendix A2, where we employ the Lagrangian Godunov-type 'meshless finite mass' (MFM) method (Hopkins 2015). The simulation suite presented in this paper is summarized in Table 1. Additional runs not included here were performed to test various numerical aspects of our simulations (fixed versus adaptive softening lengths, isotropic versus collimated outflows) as well as to expand the range of black hole parameters ($M_{\rm seed}$, $\epsilon_{\rm T}$, $v_{\rm out}$, $p_{\rm b}$; see below). The conclusions presented in this paper are not affected by any of the effects investigated in these tests, so we do not show them for brevity.

In the remainder of this section, we describe how we model black hole seeding (Section 2.1), black hole dynamics and mergers (Section 2.2), black hole accretion (Section 2.3), and black hole feedback (Section 2.4) in our simulations, as well as how we perform our main analysis (Section 2.5).

2.1 Black hole seeds

Despite much recent work, major uncertainties remain on the nature of black hole seeds (e.g. Madau & Rees 2001; Begelman, Volonteri & Rees 2006; Volonteri 2010; Choi, Shlosman & Begelman 2013). For simplicity, we do not attempt to mimic the physics of any seed formation mechanism in detail and simply assume that there is one black hole located at the centre of each galaxy when it is first resolved in the simulation. We specify the initial mass of the black hole ($M_{\rm seed}$) as well as the minimum galaxy stellar mass allowed to host a seed, $M_\star^{\rm min} = \gamma_{\rm BH} \times M_{\rm seed}$. Our approach follows Di Matteo et al. (2008). We use a Friends-of-Friends (FOF) algorithm to identify dark matter haloes during the simulation. If the FOF group does not already contain a black hole particle and its stellar mass

is $M_\star^{\rm fof} > \gamma_{\rm BH} \times M_{\rm seed}$, the gas particle with the highest density is converted into a black hole particle. For our fiducial simulations, we employ $M_{\rm seed} = 10^5\ {\rm M}_\odot\, h^{-1}$ and $\gamma_{\rm BH} = 10^3$ ($\gtrsim$15 star particles), which places black holes and galaxies approximately on the local $M_{\rm BH}$–$M_{\rm bulge}$ relation, but we vary this.

2.2 Black hole dynamics and mergers

The gravitational dynamics of black holes cannot be fully self-consistently predicted at the resolution currently achievable in cosmological simulations. Following previous work (e.g. Springel et al. 2005; Booth & Schaye 2009; Sijacki et al. 2015), we effectively fix the position of black holes to the location of the most bound particle (gas or star) within the radial aperture R_0 used to compute the accretion rate. Black hole particles are repositioned at every time step, provided that the relative velocity of the nearby most bound particle is lower than their mutual escape velocity. Different improvements to the treatment of black hole dynamics have been proposed (e.g. Wurster & Thacker 2013) but this scheme is sufficient to compute the mass growth of 'well-behaved' central black holes in our simulations. We thus assume that dynamical friction is efficient enough to maintain black holes close to the centre of galaxies but note that this may not properly capture the orbital decay of black holes in low-mass galaxies and/or at high redshift (Tremmel et al. 2015).

Galaxy merger remnants will inevitably contain two or more massive black holes that may eventually merge, but our simulations lack the resolution to follow this process in detail. Following Springel et al. (2005), we simply allow any two black holes to merge instantaneously when they are located within R_0 if their relative velocity is lower than their mutual escape velocity. We neglect the effects of gravitational recoils (Blecha et al. 2011, 2016; Sijacki, Springel & Haehnelt 2011).

2.3 Gravitational torque-driven accretion

Accretion rates are computed based on the gravitational torque model of Hopkins & Quataert (2011) as implemented in Anglés-Alcázar et al. (2013, 2015), which provides an estimate of the gas inflow rate $\dot{M}_{\rm Torque}$ driven by gravitational instabilities from galactic scales down to the accretion disc surrounding the central black hole:

$$\dot{M}_{\rm BH} = (1-\eta) \times \dot{M}_{\rm Torque}, \tag{1}$$

where we adopt a constant radiative efficiency $\eta = 0.1$ (e.g. Yu & Tremaine 2002; Marconi et al. 2004). We allow black holes to exceed the Eddington accretion rate by up to a factor of 10, but the Eddington limit itself is rarely reached in our simulations.[2] We estimate $\dot{M}_{\rm Torque}$ based on properties of the host galaxy evaluated within a distance R_0 of each black hole (Hopkins & Quataert 2011):

$$\dot{M}_{\rm Torque} \approx \epsilon_{\rm T}\, f_{\rm d}^{5/2} \times \left(\frac{M_{\rm BH}}{10^8\,{\rm M}_\odot}\right)^{1/6} \left(\frac{M_{\rm d}(R_0)}{10^9\,{\rm M}_\odot}\right) \times \left(\frac{R_0}{100\,{\rm pc}}\right)^{-3/2} \left(1+\frac{f_0}{f_{\rm gas}}\right)^{-1} {\rm M}_\odot\ {\rm yr}^{-1}, \tag{2}$$

where $f_{\rm d}$ is the disc mass fraction (including both stars and gas), $M_{\rm d}(R_0)$ is the total disc mass, $f_{\rm gas}$ is the gas mass fraction in the disc, and $f_0 \approx 0.31\ f_{\rm d}^2\ (M_{\rm d}(R_0)/10^9\,{\rm M}_\odot)^{-1/3}$.

The normalization factor $\epsilon_{\rm T}$ is intended to capture processes that affect the radial transport of gas on unresolved scales,[3] such as star formation, feedback from stars and the central black hole, and mass-loss in winds from the accretion disc, which were not modelled explicitly in Hopkins & Quataert (2011). The aperture R_0 is the distance enclosing 256 gas particles, with an upper limit of $2\,h^{-1}$ kpc (comoving) imposed throughout the simulation. Evaluating equation (2) requires separating the spheroidal and disc components of the galaxy centre, which we do by means of the same kinematic decomposition as Anglés-Alcázar et al. (2013, 2015). Numerically, black hole accretion proceeds stochastically as in Springel et al. (2005). Gas particles within R_0 can get a fraction $f_{\rm m}$ of their mass subtracted (added to the black hole) with a probability that statistically satisfies the continuous mass growth given by equation (1). A time-step limiter is imposed on black hole particles such that black holes do not grow by more than 0.1 per cent of their current mass in a single time step.

2.4 Black hole feedback

We model AGN-driven outflows by stochastically kicking particles around the black hole with velocity $v_{\rm out}$, with probability

$$p_j = \frac{1-f_{\rm m}}{f_{\rm m}} \times \frac{w_j}{m_j} \times \dot{M}_{\rm BH}\,\Delta t, \tag{3}$$

where w_j is a kernel weight ($\Sigma_j\, w_j = 1$) and $f_{\rm m}$ is the fraction of gas mass accreted by the black hole and subtracted from the gas particle before ejection. This gives an outflow mass-loading $\dot{M}_{\rm out}/\dot{M}_{\rm BH} = (1-f_{\rm m})/f_{\rm m}$. The 'momentum loading' and 'energy loading' trivially follow

$$p_{\rm b} \equiv \frac{\dot{P}_{\rm out}}{L_{\rm bol}/c} = \frac{v_{\rm out}}{\eta\, c}\left(\frac{1-f_{\rm m}}{f_{\rm m}}\right), \tag{4}$$

$$\epsilon_{\rm k} \equiv \frac{\dot{E}_{\rm out}}{L_{\rm bol}} = \frac{1}{2\,\eta}\left(\frac{v_{\rm out}}{c}\right)^2\left(\frac{1-f_{\rm m}}{f_{\rm m}}\right), \tag{5}$$

where $L_{\rm bol} = \eta\, \dot{M}_{\rm BH}\, c^2$ and c is the speed of light.

Outflowing particles are not decoupled from the hydrodynamics and cooling is not switched off for any period of time. This is similar to kinetic wind implementations used in galactic nucleus (Hopkins et al. 2016), galaxy merger (Choi et al. 2012; Debuhr et al. 2012), and cosmological 'zoom-in' simulations (Choi et al. 2015). The appropriate momentum and energy loading of winds depend on the physical scale (e.g. Faucher-Giguère & Quataert 2012). Observed properties at different radii are uncertain, so we vary $p_{\rm b}$ and $v_{\rm out}$ (see Table 1). Velocity kicks are directed radially from the black hole. We also tested a model for collimated outflows, with kicks always in the direction of the angular momentum within R_0, but we found no significant differences in quantities studied here. Similar star formation suppression efficiencies and black hole mass-to-galaxy mass ratios were obtained regardless of the outflow geometry.

[2] The 20 most massive black holes in our fiducial simulation each spend on average ∼0.1 per cent of the time accreting above the Eddington limit, which represents ∼0.3 per cent of their total mass growth through accretion. Decreasing the initial black hole seed mass by a factor of 10 increases the amount of time accreting at super-Eddington rates to ∼0.4 per cent, corresponding to ∼0.5 per cent of the overall growth.

[3] Note that $\epsilon_{\rm T} \equiv \epsilon_{\rm m} \times \alpha_{\rm T}$ in the notation adopted by Anglés-Alcázar et al. (2013, 2015), where $\epsilon_{\rm m}$ is the 'mass retention rate' and $\alpha_{\rm T}$ is the original normalization of $\dot{M}_{\rm Torque}$ in Hopkins & Quataert (2011).

2.5 Analysis of simulations

We identify dark matter haloes at each redshift snapshot by means of the Amiga Halo Finder (Gill, Knebe & Gibson 2004; Knollmann & Knebe 2009), using the evolving virial overdensity definition of Bryan & Norman (1998). Galaxies are identified independently of their parent haloes as gravitationally bound collections of gas and star particles by means of SKID,[4] where we impose a minimum density threshold for gas particles $\rho \geq 0.1$ cm^{-3} (e.g. Kereš et al. 2005). Galaxies may contain more than one black hole shortly after a galaxy merger and before the central black holes merge as well. When comparing our simulations against the observed local $M_{\rm BH}$–$M_{\rm bulge}$ relation, we add up the masses of all black holes located within the stellar effective radius ($R_{\rm e}$), which we plot against the stellar mass contained within $R_{\rm e}$ for each galaxy ($M_\star$). We repeated our analysis selecting only the most massive black hole in each galaxy. Since galaxies spend a small fraction of their time in a merging state, none of our results are significantly affected. For simplicity, we do not attempt to compute the bulge mass of galaxies in analogy with observations, but replace it instead by $M_\star$ throughout this paper. This facilitates comparisons to other numerical studies using $M_\star$ (e.g. Sijacki et al. 2015) as well as to observational studies at higher redshifts, where bulge masses are difficult to estimate. We evaluate the implications of different definitions of host galaxy bulge mass in Appendix A3, where we show that our results depend only weakly on the exact definition and our main conclusions remain unchanged.

3 THE ORIGIN OF THE $M_{\rm BH}$–$M_\star$ RELATION

Fig. 1 shows the $M_{\rm BH}$–$M_\star$ relation predicted by the gravitational torque accretion model coupled to black hole-driven outflows with velocity $v_{\rm out} = 10^3$ km s^{-1} and total momentum flux $\dot{P}_{\rm out} = L_{\rm bol}/c$. We indicate the location of individual black holes and galaxies at $z = 5$ (red circles), $z = 2$ (green triangles), and $z = 0$ (blue squares). Our fiducial simulation is in good agreement with various observational determinations of the $M_{\rm BH}$–$M_{\rm bulge}$ relation in the local universe, indicated by the grey lines. Note that we have extrapolated observed relations to the low-mass regime ($M_\star \lesssim 10^{9.5}$ M$_\odot$), where dynamical black hole mass estimates are scarce. For comparison, we also show the observed $M_{\rm BH}$–$M_\star$ relations of Reines & Volonteri (2015) for AGN and inactive galaxies separately, where $M_{\rm BH}$ is related to the total stellar mass of galaxies as opposed to the bulge mass.

Black holes with initial mass $M_{\rm seed} = 10^5$ M$_\odot$ h^{-1} were placed at the centre of galaxies as they first reached $M_\star \approx 10^3\, M_{\rm seed}$ in the simulation (i.e. roughly in agreement with the local $M_{\rm BH}$–$M_{\rm bulge}$ relation) and evolved on average along the scaling relation from early times down to $z = 0$. As we show in Section 3.2, the accretion rate normalization $\epsilon_{\rm T}$ governs the normalization of the scaling relation, while the slope arises naturally in the simulation as a consequence of the proportional growth of black holes and galaxies over cosmological time-scales. Our fiducial simulation adopts $\epsilon_{\rm T} = 0.5$, a factor of $\sim$10 lower than estimated from nuclear scale simulations without black hole feedback in Hopkins & Quataert (2011). This is within a factor of 2 to the normalization required in Anglés-Alcázar et al. (2013, 2015) to match the local $M_{\rm BH}$–$M_{\rm bulge}$ relation by post-processing cosmological simulations including star formation-driven winds but not AGN feedback (Oppenheimer & Davé 2008; Davé et al. 2013).

[4] http://www-hpcc.astro.washington.edu/tools/skid.html. We use a modified version provided as part of the SPHGR package (Thompson 2015).

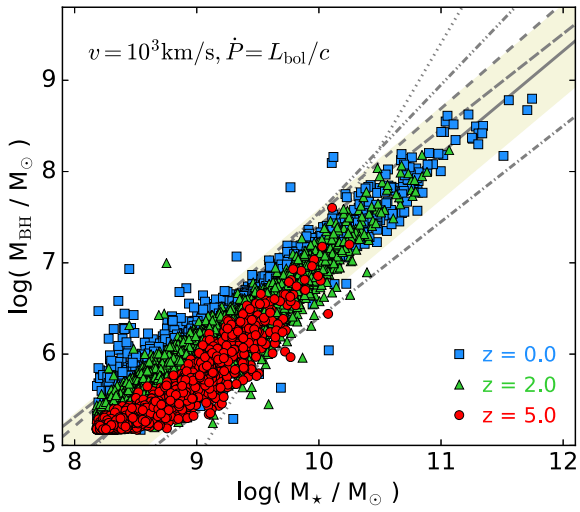

Figure 1. $M_{\rm BH}$–$M_\star$ relation at redshifts $z = 5$ (red circles), $z = 2$ (green triangles), and $z = 0$ (blue squares) for our fiducial feedback simulation. Grey lines indicate the observed local $M_{\rm BH}$–$M_{\rm bulge}$ relations of Häring & Rix (2004, solid), McConnell & Ma (2013, long dashed), Kormendy & Ho (2013, dashed), and Savorgnan et al. (2016, dotted; late-type galaxies only), and the $M_{\rm BH}$–$M_\star$ relations of Reines & Volonteri (2015) for AGN (dot–dashed) and inactive (dot–dot–dashed) samples. The beige shaded area corresponds to 0.5 dex scatter in $M_{\rm BH}$ relative to Häring & Rix (2004). Observed relations are extrapolated to lower $M_\star$ for reference. Our fiducial model (seed mass $M_{\rm seed} = 10^5$ M$_\odot$ h^{-1}, with quasar mode feedback and torque-limited accretion) agrees well with local observations and predicts no significant redshift evolution in the $M_{\rm BH}$–$M_\star$ relation.

We compute the best power-law fit to the $M_{\rm BH}$–$M_\star$ relation at each redshift in our simulations as

$$\log_{10}\left(\frac{M_{\rm BH}}{\rm M_\odot}\right) = \alpha + \beta\, \log_{10}\left(\frac{M_\star}{10^{10}\,\rm M_\odot}\right), \qquad (6)$$

where only galaxies with $M_\star > 10^{9.5}$ M$_\odot$ are included, to exclude low-mass black holes affected by our seed mass choice. Our fiducial simulation yields $\alpha \approx 7.1$ and $\beta \approx 1.1$ at $z = 0$, and we see no significant evolution in the normalization or slope of the relation.

Various observational studies differ regarding the normalization of the $M_{\rm BH}$–$M_{\rm bulge}$ relation, which may be biased by selection effects (Shankar et al. 2016). Since we show that the normalization is determined by $\epsilon_{\rm T}$ in our model (Section 3.2), we can adjust our prediction systematically by changing $\epsilon_{\rm T}$. Recent observational claims of a steeper relation $M_{\rm BH} \propto M_{\rm bulge}^2$ for black holes in late-type galaxies (Savorgnan et al. 2016) suggest that black holes may be undermassive at early times relative to their hosts. Note that early black hole growth could be delayed by complex black hole dynamics in high-redshift galaxies with chaotic morphologies, efficient stellar feedback, and other mechanisms not captured in our present simulations. In the following, we adopt the nearly linear $M_{\rm BH}$–$M_{\rm bulge}$ relation of Häring & Rix (2004) as our fiducial reference.

3.1 Effects of different seed masses

Fig. 2 shows the $M_{\rm BH}$–$M_\star$ relation at $z = 0$ for two simulations using different black hole seeds but the same accretion and feedback parameters ($v_{\rm out} = 10^3$ km s^{-1} and $\dot{P}_{\rm out} = L_{\rm bol}/c$). We introduce black hole seeds with mass $M_{\rm seed} = 10^4$ or 10^6 M$_\odot$ h^{-1} in galaxies with stellar mass $M_* > 10^8$ M$_\odot$ h^{-1} (i.e. 10 times smaller/larger

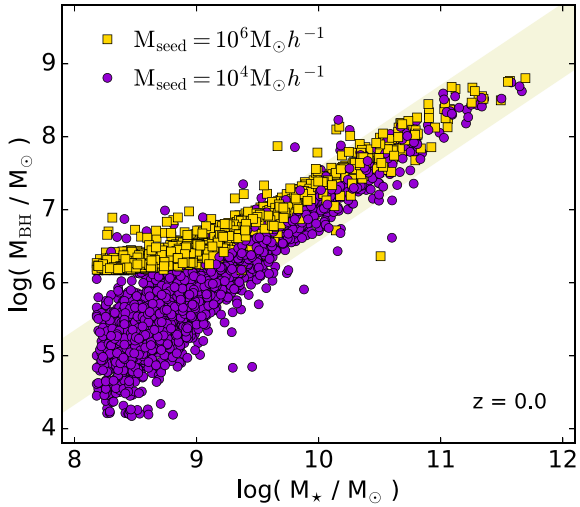

Figure 2. Effects of the black hole seed mass on the $M_{\rm BH}$–$M_\star$ relation at $z = 0$ for simulations including black hole-driven outflows with $v_{\rm out} = 10^3$ km s^{-1} and $\dot{P}_{\rm out} = L_{\rm bol}/c$. Black holes with initial mass $M_{\rm seed} = 10^6$ M$_\odot$ h^{-1}(yellow squares) and $M_{\rm seed} = 10^4$ M$_\odot$ h^{-1}(purple circles) are seeded in galaxies $M_\star > 10^8$ M$_\odot$ h^{-1}. The beige shaded area corresponds to 0.5 dex scatter in $M_{\rm BH}$ relative to Häring & Rix (2004). Because the gravitational torque accretion rate is nearly independent of $M_{\rm BH}$, black hole seeds quickly converge to the same relation.

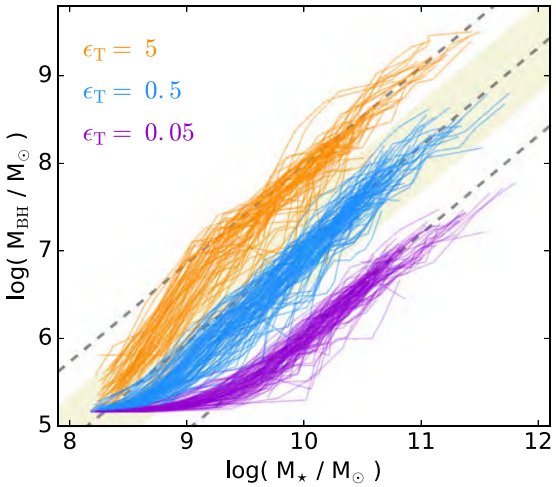

Figure 3. Effects of the black hole accretion rate normalization on the $M_{\rm BH}$–$M_\star$ relation for simulations including black hole-driven outflows with $v_{\rm out} = 10^3$ km s^{-1} and $\dot{P}_{\rm out} = L_{\rm bol}/c$. We show evolutionary tracks for the 100 most massive black holes (on the $M_{\rm BH}$–$M_\star$ plane at $z = 0$) for $\dot{M}_{\rm BH} \propto \epsilon_{\rm T} = 5$, 0.5, 0.05. Grey dashed lines indicate the Häring & Rix (2004) relation and changing its normalization up and down by a factor of 10. The accretion rate normalization $\epsilon_{\rm T}$ sets the normalization of the predicted $M_{\rm BH}$–$M_\star$ relation, with $M_{\rm BH}(M_*) \propto \epsilon_{\rm T}$.

than our default). Despite initial masses differing by two orders of magnitude, Fig. 2 shows that black holes converge on to the local relation by $z = 0$. This is in agreement with post-processing calculations that neglect the effects of black hole feedback (Anglés-Alcázar et al. 2013, 2015), suggesting that gravitational torque-driven accretion is the primary driver of the convergence. Indeed, $\dot{M}_{\rm Torque}$ is nearly independent of black hole mass (equation 2), so that the proportional growth rate $\dot{M}_{\rm BH}/M_{\rm BH} \propto M_{\rm BH}^{-5/6}$ of undermassive (overmassive) black holes is faster (slower) relative to black holes lying on the $M_{\rm BH}$–$M_\star$ relation for the same host galaxies. The time-scale for convergence on to the local relation depends on the initial $M_{\rm seed}/M_*$ ratio and redshift (Anglés-Alcázar et al. 2015), after which black holes lose memory of their seed mass.

3.2 Effects of the accretion rate normalization

Fig. 3 shows the evolutionary tracks of black holes and galaxies in the $M_{\rm BH}$–$M_\star$ plane for the 100 most massive systems in the simulated volume. We compare simulations using the same feedback parameters ($v_{\rm out} = 10^3$ km s^{-1} and $\dot{P}_{\rm out} = L_{\rm bol}/c$) but different accretion rate normalization: $\epsilon_{\rm T} = 5$ (orange), $\epsilon_{\rm T} = 0.5$ (blue), and $\epsilon_{\rm T} = 0.05$ (purple). Once $M_{\rm BH} \gg M_{\rm seed}$, we see clearly in each case that $M_{\rm BH} \propto \epsilon_{\rm T}$ for a given M_*. In other words, black holes converge on to different $M_{\rm BH}$–$M_\star$ relations corresponding to each $\epsilon_{\rm T}$. After the initial transitory growth phase, $\epsilon_{\rm T}$ controls the normalization, but not the shape, of our predicted scaling relation. This is in agreement with expectations from no-feedback calculations, where $\dot{M}_{\rm BH} \propto \epsilon_{\rm T}$ yields $M_{\rm BH} \propto \epsilon_{\rm T}$, suggesting that the linear effect of $\epsilon_{\rm T}$ on $M_{\rm BH}$ dominates over non-linear effects of black hole feedback on ∼kpc scales.

3.3 Effects of black hole feedback on the $M_{\rm BH}$–$M_\star$ relation

Fig. 4 demonstrates the impact of black hole feedback on the $M_{\rm BH}$–$M_\star$ relation by comparing simulations adopting different black

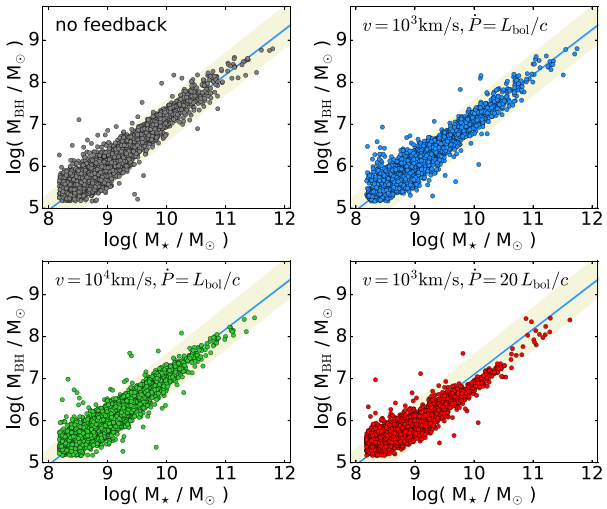

Figure 4. Effects of galaxy-scale black hole feedback on the $M_{\rm BH}$–$M_\star$ relation. We show the scaling relation obtained at $z = 0$ for simulations using different velocity ($v_{\rm out}$) and/or total momentum flux ($\dot{P}_{\rm out}$) for AGN-driven outflows coupled on ∼kpc scales, including (i) no explicit treatment of black hole feedback (top left), (ii) $v_{\rm out} = 10^3$ km s^{-1} and $\dot{P}_{\rm out} = L_{\rm bol}/c$ (top right; fiducial simulation), (iii) $v_{\rm out} = 10^4$ km s^{-1} and $\dot{P}_{\rm out} = L_{\rm bol}/c$ (bottom left), and (iv) $v_{\rm out} = 10^3$ km s^{-1} and $\dot{P}_{\rm out} = 20\,L_{\rm bol}/c$ (bottom right). All simulations use the same black hole accretion parameters. Blue solid lines indicate the best power-law fit to our fiducial $M_{\rm BH}$–$M_\star$ relation. The beige shaded area corresponds to 0.5 dex scatter in $M_{\rm BH}$ relative to Häring & Rix (2004). Although different galaxy-scale feedback choices affect both M_* and $M_{\rm BH}$ significantly, they move along the same $M_{\rm BH}$–$M_\star$ relation.

hole feedback parameters. Although different feedback choices do change both M_* and $M_{\rm BH}$ significantly (discussed further below), black holes and galaxies appear to move along the same $M_{\rm BH}$–$M_\star$ relation. The best power-law fit to our fiducial $M_{\rm BH}$–$M_\star$ relation (top right) is reproduced in all panels for comparison. Going from

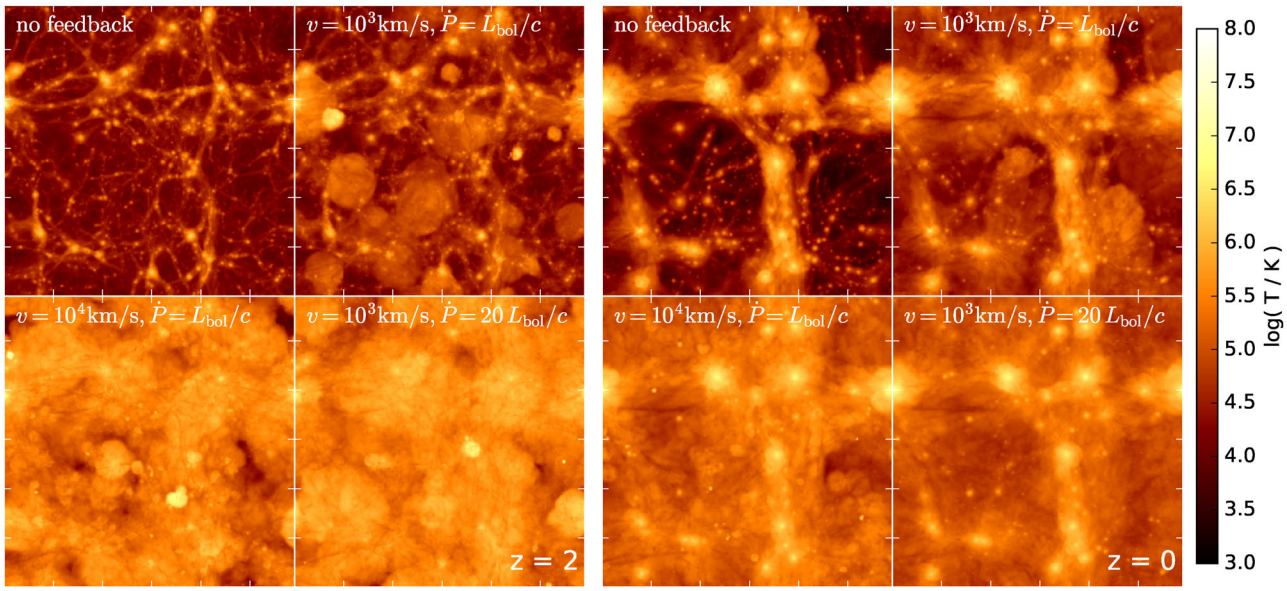

Figure 5. Mass-weighted projected temperature distributions at $z = 2$ (left) and $z = 0$ (right) for simulations with different black hole feedback strengths. For each redshift, we compare simulations including (i) no black hole feedback (top left), (ii) $v_{\rm out} = 10^3$ km s^{-1} and $\dot{P}_{\rm out} = L_{\rm bol}/c$ (top right; fiducial simulation), (iii) $v_{\rm out} = 10^4$ km s^{-1} and $\dot{P}_{\rm out} = L_{\rm bol}/c$ (bottom left), and (iv) $v_{\rm out} = 10^3$ km s^{-1} and $\dot{P}_{\rm out} = 20\,L_{\rm bol}/c$ (bottom right). Each panel represents the full simulated volume, i.e. $20\,h^{-1}$ Mpc comoving on a side. Black hole feedback strongly affects the thermal properties of the intergalactic medium for the range of feedback parameters considered, including kinetic efficiencies $\epsilon_{\rm k}$ as low as 10^{-3} and momentum-loading $p_{\rm b}$ as low as 1.

the no-feedback simulation (top left) to our strongest feedback case ($v_{\rm out} = 10^3$ km s^{-1}, $\dot{P}_{\rm out} = 20\,L_{\rm bol}/c$; bottom right), $M_{\rm BH}(M_*)$ decreases by only a factor of $\sim$2 for black holes in $M_\star \sim 10^{10}$ M$_\odot$ galaxies. Overall, all simulations are in good agreement with the observed relation, suggesting that galaxy-scale black hole feedback does not play a primary role in establishing the scaling relations.

4 EFFECTS OF BLACK HOLE FEEDBACK ON GALAXIES AND THE IGM

We now examine the impact of black hole feedback on properties other than the $M_{\rm BH}$–$M_\star$ relation.

4.1 Thermal properties of the intergalactic medium

Fig. 5 illustrates the impact of black hole feedback on cosmological scales by showing the projected (mass-weighted) gas temperature distribution at $z = 2$ and 0. As in Fig. 4, we compare simulations with different feedback parameters. In the absence of black hole feedback, the main heating sources of the intergalactic medium in our simulations are the photoionizing background and virial shocks that develop as gas accretes on to dark matter haloes.

The impact of black hole feedback on the thermal properties of the intergalactic medium is evident already at $z = 2$ in our fiducial simulation. Black hole-driven outflows create bubbles of hot gas expanding over scales significantly larger than the host dark matter haloes. The effects of black hole feedback on large scales become even more dramatic when we increase the outflow velocity to $v_{\rm out} = 10^4$ km s^{-1}: a significant portion of the IGM is heated to temperatures $\gtrsim 10^6$ K. Similar large-scale effects are seen for $v_{\rm out} = 10^3$ km s^{-1} and $\dot{P}_{\rm out} = 20\,L_{\rm bol}/c$.

We quantify in Fig. 6 the efficiency of black hole feedback heating by showing mass-weighted temperature distributions for the gas within the virial radius of dark matter haloes (dashed lines) and outside of haloes (solid lines) at $z = 0$. Only gas particles with

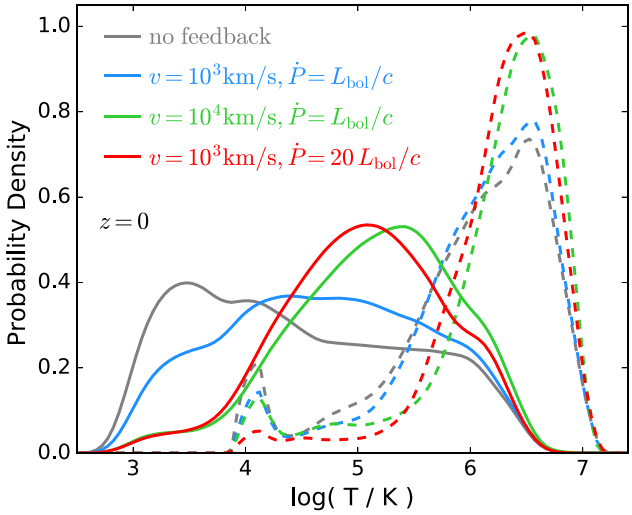

Figure 6. Mass-weighted probability distribution for the temperature of the gas within haloes (ignoring star-forming gas; dashed lines) and outside of haloes (solid lines) at $z = 0$ for simulations with different feedback parameters, including (i) no black hole feedback (grey), (ii) $v_{\rm out} = 10^3$ km s^{-1} and $\dot{P}_{\rm out} = L_{\rm bol}/c$ (blue; fiducial simulation), (iii) $v_{\rm out} = 10^4$ km s^{-1} and $\dot{P}_{\rm out} = L_{\rm bol}/c$ (green), and (iv) $v_{\rm out} = 10^3$ km s^{-1} and $\dot{P}_{\rm out} = 20\,L_{\rm bol}/c$ (red). Inside massive haloes, virial shocks dominate heating and black hole feedback is a secondary effect. Outside haloes, fast black hole-driven winds can increase the IGM temperature by factors of $\sim$3–10.

density below the threshold for star formation are included ($n_{\rm H} \lesssim 0.13$ cm^{-3}). The temperature distribution of gas within haloes is shifted towards higher temperatures in simulations with black hole feedback, where the median temperature increases by $\sim$15 per cent, 70 per cent, and 60 per cent relative to the no-feedback simulation for our fiducial, high-velocity ($v_{\rm out} = 10^4$ km s^{-1}), and large momentum boost ($\dot{P}_{\rm out} = 20\,L_{\rm bol}/c$) simulations, respectively. As

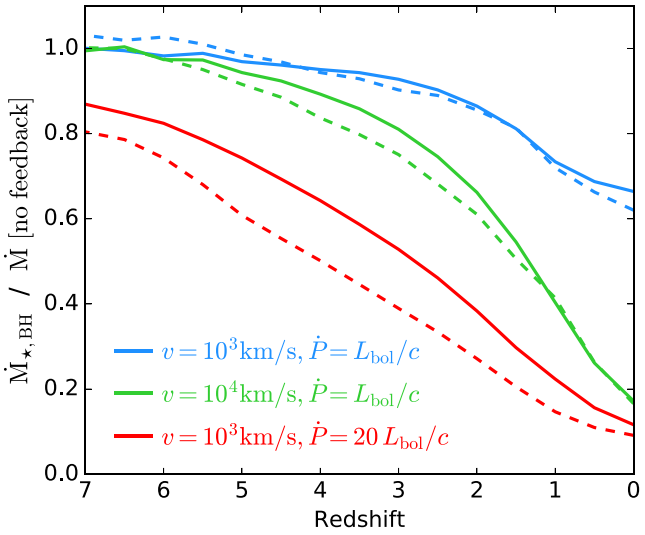

Figure 7. Impact of galaxy-scale black hole feedback on the global growth of black holes and galaxies. We show the volume-integrated SFR (solid lines) and black hole growth rate (dashed lines), normalized to the corresponding rates in our no-feedback simulation. We compare simulations with outflow velocity and total momentum flux (i) $v_{\rm out} = 10^3$ km s^{-1} and $\dot{P}_{\rm out} = L_{\rm bol}/c$ (blue; fiducial simulation), (ii) $v_{\rm out} = 10^4$ km s^{-1} and $\dot{P}_{\rm out} = L_{\rm bol}/c$ (green), and (iii) $v_{\rm out} = 10^3$ km s^{-1} and $\dot{P}_{\rm out} = 20\,L_{\rm bol}/c$ (red). Black hole-driven outflows reduce the SFR and black hole accretion rate by a similar amount, increasingly so for simulations with higher feedback efficiency and lower redshift.

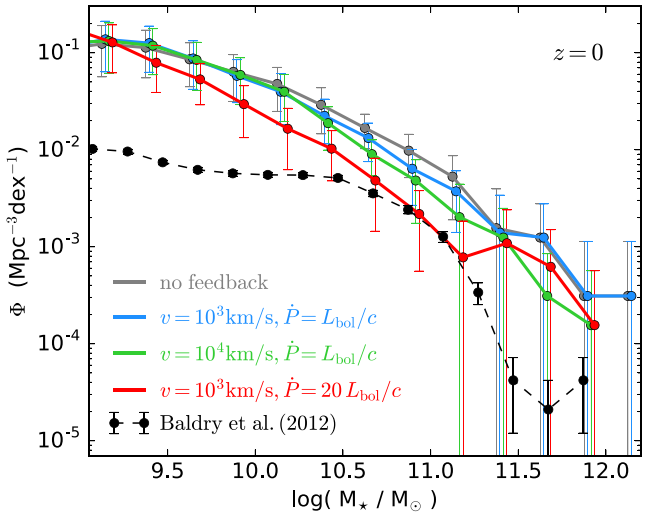

Figure 8. Galaxy stellar mass function at $z = 0$ for simulations with different black hole feedback parameters, including (i) no feedback (grey), (ii) $v_{\rm out} = 10^3$ km s^{-1} and $\dot{P}_{\rm out} = L_{\rm bol}/c$ (blue; fiducial simulation), (iii) $v_{\rm out} = 10^4$ km s^{-1} and $\dot{P}_{\rm out} = L_{\rm bol}/c$ (green), and (iv) $v_{\rm out} = 10^3$ km s^{-1} and $\dot{P}_{\rm out} = 20\,L_{\rm bol}/c$ (red). Error bars show cosmic variance estimates computed as the standard deviation over the eight sub-octants of the simulated volume. Black points connected by a dashed line show the observed stellar mass function from Baldry et al. (2012). Quasar mode feedback alone is not sufficient to reproduce the observed galaxy mass function, either at low or high masses.

expected from Fig. 5, the relative impact of black hole feedback on gas at larger scales is more prominent. The median temperature of gas outside of haloes increases by roughly one order of magnitude from no-feedback to our high-velocity and large momentum boost simulations.

4.2 Global stellar and black hole growth

Fig. 7 shows the effect of black hole feedback on the volume-integrated mass growth in stars and black holes at different redshifts. Our fiducial feedback parameters yield a modest but systematic decrease in the total star formation and black hole growth rate relative to the no-feedback simulation, most noticeable at $z \lesssim 2$. The effects are weaker at high redshift because (1) black holes are just seeded, and not yet massive, and (2) galaxies are mostly low-mass, where black hole feedback is weak. As expected, increasing the energy or momentum loading of outflows increases these effects. For our high-velocity ($v_{\rm out} = 10^4$ km s^{-1}) and large momentum boost ($\dot{P}_{\rm out} = 20\,L_{\rm bol}/c$) simulations, the volume-integrated SFR and black hole accretion rate are reduced by a factor of ∼5–10 at $z = 0$. Galaxy-scale AGN feedback suppresses global stellar and black hole growth by similar amounts, maintaining the slope of the $M_{\rm BH}$–$M_\star$ relation but leading to the reduction in the number of systems at the high-mass end in Fig. 4.

4.3 Galaxy stellar mass function

Fig. 8 shows the stellar mass function at $z = 0$ for simulations with different black hole feedback strengths. As expected, the no-feedback simulation greatly overpredicts the number of galaxies at all masses owing to the lack of star formation-driven winds (e.g. Oppenheimer et al. 2010; Davé et al. 2011a). Our fiducial black hole feedback parameters ($v_{\rm out} = 10^3$ km s^{-1} and $\dot{P}_{\rm out} = L_{\rm bol}/c$) yield a modest decrease in the number density of galaxies around the knee of the distribution. Higher velocity outflows ($v_{\rm out} = 10^4$ km s^{-1}) yield a stronger suppression of the stellar mass function extending to higher galaxy masses. Our large momentum boost simulation ($\dot{P}_{\rm out} = 20\,L_{\rm bol}/c$) reproduces the observed number density of galaxies around the knee of the distribution but black hole feedback alone fails to reproduce the stellar mass function at both lower and higher masses. AGN-driven outflows can thus have a significant impact on the galaxy stellar mass function but cannot replace the effects of stellar feedback in the low-mass regime. From our experiments, we cannot yet conclusively determine whether AGN feedback can quench high-mass galaxies because this requires us to correctly model the properties of lower mass galaxies that grow and merge into more massive systems. We will address this question in future simulations including a realistic model for stellar feedback.

4.4 Mass dependence of black hole feedback effects

Fig. 9 shows in more detail how the effects of black hole feedback depend on galaxy stellar mass. We cross-match galaxies between simulations based on the unique ID of the particles they contain at $z = 0$. Each galaxy is matched to the galaxy that contains the largest number of common star particles, which we use to compute the stellar mass of galaxies in simulations with black hole feedback relative to the no-feedback simulation.

Black hole feedback in our simulations with $v_{\rm out} = 10^3$ km s^{-1} is more effective at suppressing star formation and black hole growth in galaxies in the mass range $M_\star \approx 10^9$–10^{11} M$_\odot$ at $z = 0$. This trend with $M_\star$, already present at $z = 2$, suggests that black holes in lower mass galaxies have not coupled enough energy to affect their host galaxies from the time of seeding down to $z = 0$ (which may be sensitive to our seed model), while outflows with $v_{\rm out} = 10^3$ km s^{-1} may not be sufficient to unbind gas in galaxies at the highest masses.

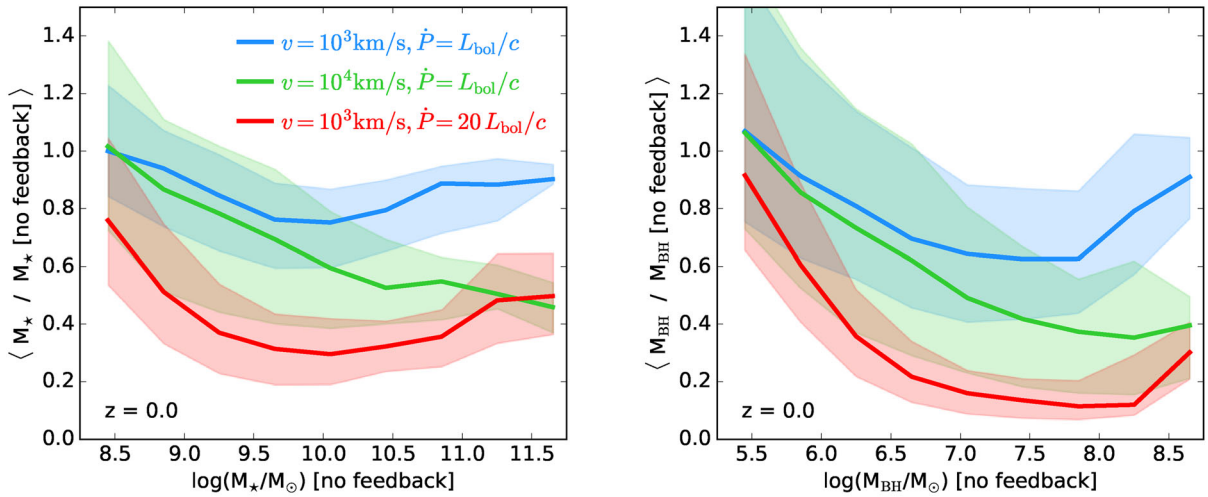

Figure 9. Mass-dependent effects of galaxy-scale black hole feedback. Left: ratio of the stellar mass of galaxies at $z = 0$ in simulations including black hole feedback to the stellar mass of the corresponding galaxies in the no-feedback simulation as a function of stellar mass. Different colours indicate simulations with different outflow velocity and momentum flux. Solid lines and shaded regions indicate median and 10 per cent–90 per cent percentile ranges. Right: same as left for black hole masses. Black hole feedback appears to be more effective in galaxies with mass $M_\star \sim 10^{10}$ M$_\odot$ for outflows with velocity $v_{\rm out} = 10^3$ km s^{-1}, while the mass suppression efficiency increases to higher mass galaxies for simulations with $v_{\rm out} = 10^4$ km s^{-1}. The overall effect of feedback on the growth of black holes and galaxies is qualitatively similar.

With the same momentum flux and $v_{\rm out} = 10^4$ km s^{-1}, the results are similar at low M_* but the mass suppression efficiency keeps increasing towards high masses, giving a ∼60 per cent reduction of the stellar mass of galaxies with $M_\star \gtrsim 10^{11.5}$ M$_\odot$ by $z = 0$. As expected, our simulation with $v_{\rm out} = 10^3$ km s^{-1} and $\dot{P}_{\rm out} = 20\,L_{\rm bol}/c$ yields the strongest suppression of stellar growth at all masses, but the efficiency follows a trend with $M_\star$ similar to that of the fiducial simulation. Black holes suppress their own growth with increasing efficiency towards higher masses roughly in a similar way as they suppress the growth of their host galaxies. Thus, the $M_{\rm BH}$–$M_\star$ relation is roughly preserved.

5 DISCUSSION

We have implemented a self-consistent black hole growth model into the GIZMO code based on the analytic gravitational torque mass inflow rate of Hopkins & Quataert (2011). This model captures the key scalings governing angular momentum transport from galactic scales down to parsec scales and reproduces the average gas inflow rates found in idealized nuclear scale simulations (Hopkins & Quataert 2010; Hopkins et al. 2016). We have further implemented a kinetic black hole feedback model coupled to accretion. This model does not attempt to explicitly capture wind driving mechanisms, but builds on previous kinetic feedback implementations in the literature applied to nuclear scale simulations (Hopkins et al. 2016), galaxy merger simulations (Choi et al. 2012; Debuhr et al. 2012), and cosmological 'zoom-in' simulations (Choi et al. 2015). In large-volume cosmological simulations, we explore the effects of outflows with parameters similar to observed fast nuclear outflows ($v_{\rm out} = 10^4$ km s^{-1}, $\dot{P}_{\rm out} = L_{\rm bol}/c$; e.g. Tombesi et al. 2013; Nardini et al. 2015) and galaxy-scale AGN-driven winds ($v_{\rm out} = 10^3$ km s^{-1}, $\dot{P}_{\rm out} = 20\,L_{\rm bol}/c$; e.g. Faucher-Giguère & Quataert 2012; Faucher-Giguère, Quataert & Murray 2012; Cicone et al. 2014; Harrison et al. 2014; Stern et al. 2016).

Our simulations show that black hole feedback can have a large impact on the thermodynamic properties of the intergalactic medium as well as the overall growth of galaxies and massive black holes, in qualitative agreement with previous work (e.g. Sijacki et al. 2007; Vogelsberger et al. 2014; Schaye et al. 2015). Relative to our no-feedback simulation, black hole-driven outflows yield a reduction in the total production of stars in the simulated volume by $z = 0$ of ∼20 per cent, 40 per cent, and 60 per cent for our fiducial, high-velocity ($v_{\rm out} = 10^4$ km s^{-1}), and large momentum boost ($\dot{P}_{\rm out} = 20\,L_{\rm bol}/c$) simulations, respectively. These correspond to momentum-loading factors (1, 1, 20) $L_{\rm bol}/c$ and energy-loading factors (0.1, 1, 3) per cent $L_{\rm bol}$. Kinetic AGN outflows can thus have a large impact even for energetic efficiencies as low as 0.1 per cent $L_{\rm bol}$ (Hopkins & Elvis 2010). Black holes suppress their own growth by similar, somewhat larger, factors, preserving the black hole–host scaling relations.

The gravitational torque accretion model has several important consequences. Because the inflow rate from this mechanism is approximately proportional to the nuclear gas supply, a linear black hole–host mass scaling emerges naturally (with slope and scatter in good agreement with that observed), *independent* of galaxy-scale black hole feedback (Anglés-Alcázar et al. 2013, 2015; see also Cen 2015). Although black hole feedback on ∼kpc scales does suppress both black hole growth and galaxy growth, removing gas from large-scale reservoirs suppresses both by a similar amount, moving systems along (not off) the scaling relations. In short, black hole and central galaxy mass are determined by a common gas supply modulated by gravitational torques, as increasingly suggested by observations of AGN in star-forming galaxies (e.g. Rafferty et al. 2011; Mullaney et al. 2012; Chen et al. 2013; Rosario et al. 2013; Trump et al. 2013, 2015; Heckman & Best 2014; Hickox et al. 2014; Vito et al. 2014; Dai et al. 2015; Delvecchio et al. 2015; Sabater, Best & Heckman 2015; Sun et al. 2015). Because the black hole fuelling rate is determined by gravitational instabilities and resulting torques, it is nearly independent of black hole mass. This in turn means that the black hole–host scaling relations are insensitive to the 'seed' black hole mass. Undermassive and overmassive black holes grow proportionally faster and slower than their host galaxies, respectively, converging on to the scaling relations without the need for self-regulation by galaxy-scale feedback (Anglés-Alcázar et al.

2013). Similar convergence may be indicated by recent observations of accreting black holes in star-forming galaxies at $z \lesssim 2$ (Sun et al. 2015; see also Merloni et al. 2010). Merging of galaxies and central black holes may help reduce the scatter of the scaling relations (Peng 2007; Hirschmann et al. 2010; Jahnke & Macciò 2011) but we find that it is not a significant contribution (Anglés-Alcázar et al. 2015).

In our simulations, the normalization of the black hole–host relation is controlled by the normalization of the mean accretion rate from $\sim$ kpc scales down to the black hole ($\epsilon_{\rm T}$). To match the $z = 0$ observed scaling relation, we require a factor of $\sim$10 lower $\epsilon_{\rm T}$ than the inflow rate down to $\sim$ pc scales estimated in Hopkins & Quataert (2011). Several processes can potentially suppress black hole accretion relative to the inflowing gas driven by gravitational torques, such as mass-loss in winds from the accretion disc (Anglés-Alcázar et al. 2015) or due to stellar feedback in the galactic nucleus, which were not modelled in Hopkins & Quataert (2011). Our lower normalization $\epsilon_{\rm T}$ can thus be interpreted as approximating the net effect of such processes. More recent simulations in Hopkins et al. (2016) showed that accretion-disc winds coupling to the gas on small scales can vent some hot, fast material to large scales (the galaxy-scale black hole feedback modelled here), while driving slower outflows in the cold, dense gas forming the high-column-density (e.g. torus) regions at $\lesssim$100 pc. The latter do not escape the galaxy centre, but can suppress accretion by a factor of $\sim$10 by evacuating gas from the vicinity of the black hole. In this sense, black hole feedback on small scales may still play a significant role in determining the normalization of the scaling relations. In our models, $\epsilon_{\rm T}$ is independent of redshift, which yields redshift-independent black hole–host correlations. However, given systematic redshift evolution in average Eddington ratios (Anglés-Alcázar et al. 2015) and the typical densities, metallicities, and SFR properties in galactic nuclei, it is plausible that $\epsilon_{\rm T}$ (hence the black hole–host scalings) could evolve (see, e.g., Hopkins et al. 2007a; Di Matteo et al. 2008; DeGraf et al. 2015; Sijacki et al. 2015). Observations remain inconclusive regarding such evolution (e.g. Trakhtenbrot & Netzer 2010; Bongiorno et al. 2014; Schulze & Wisotzki 2014; Shen et al. 2015; Sun et al. 2015; Willott, Bergeron & Omont 2015).

In this study, we have deliberately simplified the complexity of galaxy formation physics in our simulations to isolate the effects of black holes and make large-volume simulations more feasible. Our simulations utilize the sub-grid model of Springel & Hernquist (2003) instead of resolving a multi-phase interstellar medium (ISM) and do not include stellar feedback-driven winds (e.g. Davé et al. 2011a,b; Agertz et al. 2013; Anglés-Alcázar et al. 2014; Hopkins et al. 2014). The impact of black hole feedback at galactic scales may depend on these properties (e.g. Gabor & Bournaud 2014; Hopkins et al. 2016; Roos et al. 2015), which will be considered in future work. The gravitational torque model predicts the inflow rates measured in nuclear scale simulations including detailed stellar feedback processes significantly better than other models (Hopkins et al. 2016). None the less, additional mechanisms for angular momentum transport (e.g. scattering of dense gas clumps and gravitational instability-driven turbulence) should be considered in regimes where it may not be appropriate (Hopkins & Quataert 2011).

6 CONCLUSIONS

Modelling black hole growth and feedback in a cosmological context continues to be a significant challenge even in the latest cosmological hydrodynamical simulations. The models presented here emphasize (1) the importance of gravitational torques regulating a common gas supply for star formation and black hole growth and (2) the potential impact of AGN-driven outflows on galaxy evolution. Our results suggest that the efficiency with which gravitational torques feed the central black hole relative to the host galaxy SFR plays a primary role in the observed connection between massive black holes and galaxies, while the scaling relations are relatively insensitive to the amount of black hole feedback injected at galactic scales. This highlights the importance of using observations other than the scaling relations to constrain black hole feedback models, including direct measurements of outflow properties and the thermodynamic state of gas in the intergalactic medium. In future work, we will extend this study to higher resolution simulations with more realistic ISM physics to investigate whether our main conclusions continue to hold as physical processes operating below the resolution of our present cosmological simulations are explicitly resolved.

ACKNOWLEDGEMENTS

We thank M. Elitzur, E. Quataert, and P. Torrey for useful discussions and M. van Daalen for providing the initial conditions. We also thank the referee for constructive comments that helped improve the paper. DAA acknowledges support by a CIERA Postdoctoral Fellowship. RD acknowledges support from the South African Research Chairs Initiative and the South African National Research Foundation, and funding from NASA ATP grant NNX12AH86G to the University of Arizona. CAFG was supported by NSF through grants AST-1412836 and AST-1517491, by NASA through grant NNX15AB22G, and by STScI through grants HST-AR-14293.001-A and HST-GO-14268.022-A. FÖ acknowledges support from NSF grant AST-1108753 and NASA TCAN award NNX14AB48G. Support for PFH was provided by an Alfred P. Sloan Research Fellowship, NASA ATP Grant NNX14AH35G, and NSF Collaborative Research Grant #1411920 and CAREER grant #1455342. Numerical calculations were run using Northwestern University's compute cluster 'Quest' and the Extreme Science and Engineering Discovery Environment (XSEDE), which is supported by NSF grant ACI-1053575. This work benefited from the hospitality of the Aspen Center for Physics, supported by NSF grant PHY-1066293.

REFERENCES

Abadi M. G., Navarro J. F., Steinmetz M., Eke V. R., 2003, ApJ, 597, 21
Agertz O., Kravtsov A. V., Leitner S. N., Gnedin N. Y., 2013, ApJ, 770, 25
Anglés-Alcázar D., Özel F., Davé R., 2013, ApJ, 770, 5
Anglés-Alcázar D., Davé R., Özel F., Oppenheimer B. D., 2014, ApJ, 782, 84
Anglés-Alcázar D., Özel F., Davé R., Katz N., Kollmeier J. A., Oppenheimer B. D., 2015, ApJ, 800, 127
Baldry I. K. et al., 2012, MNRAS, 421, 621
Begelman M. C., Volonteri M., Rees M. J., 2006, MNRAS, 370, 289
Blecha L., Cox T. J., Loeb A., Hernquist L., 2011, MNRAS, 412, 2154
Blecha L. et al., 2016, MNRAS, 456, 961
Bondi H., 1952, MNRAS, 112, 195
Bondi H., Hoyle F., 1944, MNRAS, 104, 273
Bongiorno A. et al., 2014, MNRAS, 443, 2077
Booth C. M., Schaye J., 2009, MNRAS, 398, 53
Bournaud F., Dekel A., Teyssier R., Cacciato M., Daddi E., Juneau S., Shankar F., 2011, ApJ, 741, L33
Bourne M. A., Zubovas K., Nayakshin S., 2015, MNRAS, 453, 1829
Brooks A. M., Christensen C. R., 2016, Astrophysics and Space Science Library, Vol. 418, Galactic Bulges. Springer, Berlin, p. 317

Bryan G. L., Norman M. L., 1998, ApJ, 495, 80
Cattaneo A. et al., 2009, Nature, 460, 213
Cen R., 2015, ApJ, 805, L9
Chen C.-T. J. et al., 2013, ApJ, 773, 3
Choi E., Ostriker J. P., Naab T., Johansson P. H., 2012, ApJ, 754, 125
Choi E., Ostriker J. P., Naab T., Oser L., Moster B. P., 2015, MNRAS, 449, 4105
Choi J.-H., Shlosman I., Begelman M. C., 2013, ApJ, 774, 149
Cicone C. et al., 2014, A&A, 562, A21
Dai Y. S., Wilkes B. J., Bergeron J., Omont A., Kuraszkiewicz J., Teplitz H. I., 2015, preprint (arXiv:1511.06761)
Davé R., Oppenheimer B. D., Finlator K., 2011a, MNRAS, 415, 11
Davé R., Finlator K., Oppenheimer B. D., 2011b, MNRAS, 416, 1354
Davé R., Katz N., Oppenheimer B. D., Kollmeier J. A., Weinberg D. H., 2013, MNRAS, 434, 2645
Debuhr J., Quataert E., Ma C.-P., 2012, MNRAS, 420, 2221
DeGraf C., Di Matteo T., Treu T., Feng Y., Woo J.-H., Park D., 2015, MNRAS, 454, 913
Delvecchio I. et al., 2015, MNRAS, 449, 373
Di Matteo T., Springel V., Hernquist L., 2005, Nature, 433, 604
Di Matteo T., Colberg J., Springel V., Hernquist L., Sijacki D., 2008, ApJ, 676, 33
Dubois Y., Devriendt J., Slyz A., Teyssier R., 2012, MNRAS, 420, 2662
Durier F., Dalla Vecchia C., 2012, MNRAS, 419, 465
Escala A., 2007, ApJ, 671, 1264
Fabian A. C., 2012, ARA&A, 50, 455
Faucher-Giguère C.-A., Quataert E., 2012, MNRAS, 425, 605
Faucher-Giguère C.-A., Lidz A., Zaldarriaga M., Hernquist L., 2009, ApJ, 703, 1416
Faucher-Giguère C.-A., Quataert E., Murray N., 2012, MNRAS, 420, 1347
Feruglio C., Maiolino R., Piconcelli E., Menci N., Aussel H., Lamastra A., Fiore F., 2010, A&A, 518, L155
Filloux C., Durier F., Pacheco J. A. F., Silk J., 2010, Int. J. Mod. Phys. D, 19, 1233
Gabor J. M., Bournaud F., 2014, MNRAS, 441, 1615
Gill S. P. D., Knebe A., Gibson B. K., 2004, MNRAS, 351, 399
Graham A. W., Scott N., 2013, ApJ, 764, 151
Greene J. E., Zakamska N. L., Smith P. S., 2012, ApJ, 746, 86
Gültekin K. et al., 2009, ApJ, 698, 198
Hahn O., Abel T., 2011, MNRAS, 415, 2101
Häring N., Rix H.-W., 2004, ApJ, 604, L89
Harrison C. M., Alexander D. M., Mullaney J. R., Swinbank A. M., 2014, MNRAS, 441, 3306
Heckman T. M., Best P. N., 2014, ARA&A, 52, 589
Hernquist L., 1989, Nature, 340, 687
Hickox R. C., Mullaney J. R., Alexander D. M., Chen C.-T. J., Civano F. M., Goulding A. D., Hainline K. N., 2014, ApJ, 782, 9
Hirschmann M., Khochfar S., Burkert A., Naab T., Genel S., Somerville R. S., 2010, MNRAS, 407, 1016
Hopkins P. F., 2013, MNRAS, 428, 2840
Hopkins P. F., 2015, MNRAS, 450, 53
Hopkins P. F., Elvis M., 2010, MNRAS, 401, 7
Hopkins P. F., Quataert E., 2010, MNRAS, 407, 1529
Hopkins P. F., Quataert E., 2011, MNRAS, 415, 1027
Hopkins P. F., Hernquist L., Cox T. J., Di Matteo T., Martini P., Robertson B., Springel V., 2005, ApJ, 630, 705
Hopkins P. F., Hernquist L., Cox T. J., Di Matteo T., Robertson B., Springel V., 2006, ApJS, 163, 1
Hopkins P. F., Hernquist L., Cox T. J., Robertson B., Krause E., 2007a, ApJ, 669, 45
Hopkins P. F., Hernquist L., Cox T. J., Robertson B., Krause E., 2007b, ApJ, 669, 67
Hopkins P. F., Kereš D., Oñorbe J., Faucher-Giguère C.-A., Quataert E., Murray N., Bullock J. S., 2014, MNRAS, 445, 581
Hopkins P. F., Torrey P., Faucher-Giguere C.-A., Quataert E., Murray N., 2016, MNRAS, 458, 816
Jahnke K., Macciò A. V., 2011, ApJ, 734, 92
Jahnke K. et al., 2009, ApJ, 706, L215
Jogee S., 2006, in Alloin D., ed., Lecture Notes in Physics, Vol. 693, Physics of Active Galactic Nuclei at All Scales. Springer-Verlag, Berlin, p. 143
Katz N., Weinberg D. H., Hernquist L., 1996, ApJS, 105, 19
Kennicutt R. C., Jr, 1998, ApJ, 498, 541
Kereš D., Katz N., Weinberg D. H., Davé R., 2005, MNRAS, 363, 2
King A., 2003, ApJ, 596, L27
King A., Pounds K., 2015, ARA&A, 53, 115
Knollmann S. R., Knebe A., 2009, ApJS, 182, 608
Kormendy J., Ho L. C., 2013, ARA&A, 51, 511
Levine R., Gnedin N. Y., Hamilton A. J. S., Kravtsov A. V., 2008, ApJ, 678, 154
Liu G., Zakamska N. L., Greene J. E., Nesvadba N. P. H., Liu X., 2013, MNRAS, 436, 2576
McConnell N. J., Ma C.-P., 2013, ApJ, 764, 184
McKee C. F., Ostriker J. P., 1977, ApJ, 218, 148
Madau P., Rees M. J., 2001, ApJ, 551, L27
Maiolino R. et al., 2012, MNRAS, 425, L66
Marconi A., Risaliti G., Gilli R., Hunt L. K., Maiolino R., Salvati M., 2004, MNRAS, 351, 169
Merloni A. et al., 2010, ApJ, 708, 137
Mullaney J. R. et al., 2012, ApJ, 753, L30
Murray N., Quataert E., Thompson T. A., 2005, ApJ, 618, 569
Nardini E. et al., 2015, Science, 347, 860
Oppenheimer B. D., Davé R., 2008, MNRAS, 387, 577
Oppenheimer B. D., Davé R., Kereš D., Fardal M., Katz N., Kollmeier J. A., Weinberg D. H., 2010, MNRAS, 406, 2325
Peng C. Y., 2007, ApJ, 671, 1098
Planck Collaboration XIII, 2016, A&A, 594, A13
Price D. J., Monaghan J. J., 2007, MNRAS, 374, 1347
Rafferty D. A., Brandt W. N., Alexander D. M., Xue Y. Q., Bauer F. E., Lehmer B. D., Luo B., Papovich C., 2011, ApJ, 742, 3
Reines A. E., Volonteri M., 2015, ApJ, 813, 82
Roos O., Juneau S., Bournaud F., Gabor J. M., 2015, ApJ, 800, 19
Rosario D. J. et al., 2013, ApJ, 771, 63
Rosas-Guevara Y. M. et al., 2015, MNRAS, 454, 1038
Rupke D. S. N., Veilleux S., 2011, ApJ, 729, L27
Sabater J., Best P. N., Heckman T. M., 2015, MNRAS, 447, 110
Saitoh T. R., Makino J., 2013, ApJ, 768, 44
Savorgnan G. A. D., Graham A. W., Marconi A., Sani E., 2016, ApJ, 817, 21
Schaye J. et al., 2015, MNRAS, 446, 521
Schmidt M., 1959, ApJ, 129, 243
Schulze A., Wisotzki L., 2014, MNRAS, 438, 3422
Shankar F. et al., 2016, MNRAS, 460, 3119
Shen Y. et al., 2015, ApJ, 805, 96
Shlosman I., Frank J., Begelman M. C., 1989, Nature, 338, 45
Shlosman I., Begelman M. C., Frank J., 1990, Nature, 345, 679
Sijacki D., Springel V., Di Matteo T., Hernquist L., 2007, MNRAS, 380, 877
Sijacki D., Springel V., Haehnelt M. G., 2011, MNRAS, 414, 3656
Sijacki D., Vogelsberger M., Genel S., Springel V., Torrey P., Snyder G. F., Nelson D., Hernquist L., 2015, MNRAS, 452, 575
Silk J., Rees M. J., 1998, A&A, 331, L1
Soltan A., 1982, MNRAS, 200, 115
Somerville R. S., Davé R., 2015, ARA&A, 53, 51
Somerville R. S., Hopkins P. F., Cox T. J., Robertson B. E., Hernquist L., 2008, MNRAS, 391, 481
Springel V., 2005, MNRAS, 364, 1105
Springel V., Hernquist L., 2003, MNRAS, 339, 289
Springel V., Di Matteo T., Hernquist L., 2005, MNRAS, 361, 776
Steinborn L. K., Dolag K., Hirschmann M., Prieto M. A., Remus R.-S., 2015, MNRAS, 448, 1504
Stern J., Faucher-Giguere C.-A., Zakamska N. L., Hennawi J. F., 2016, ApJ, 819, 130
Sturm E. et al., 2011, ApJ, 733, L16
Sun M. et al., 2015, ApJ, 802, 14
Thompson R., 2015, Astrophysics Source Code Library, record ascl:1502.012

Tombesi F., Cappi M., Reeves J. N., Nemmen R. S., Braito V., Gaspari M., Reynolds C. S., 2013, MNRAS, 430, 1102
Trakhtenbrot B., Netzer H., 2010, MNRAS, 406, L35
Tremmel M., Governato F., Volonteri M., Quinn T. R., 2015, MNRAS, 451, 1868
Trump J. R., Hsu A. D., Fang J. J., Faber S. M., Koo D. C., Kocevski D. D., 2013, ApJ, 763, 133
Trump J. R. et al., 2015, ApJ, 811, 26
van den Bosch R., 2016, preprint (arXiv:1606.01246)
Vito F. et al., 2014, MNRAS, 441, 1059
Vogelsberger M. et al., 2014, MNRAS, 444, 1518
Volonteri M., 2010, A&AR, 18, 279
Wiersma R. P. C., Schaye J., Smith B. D., 2009, MNRAS, 393, 99
Willott C. J., Bergeron J., Omont A., 2015, ApJ, 801, 123
Woo J.-H., Schulze A., Park D., Kang W.-R., Kim S. C., Riechers D. A., 2013, ApJ, 772, 49
Wurster J., Thacker R. J., 2013, MNRAS, 431, 2513
Yu Q., Tremaine S., 2002, MNRAS, 335, 965

APPENDIX A: NUMERICAL ROBUSTNESS

Different aspects of the numerical robustness of our gravitational torque accretion model have been discussed in Anglés-Alcázar et al. (2013, 2015). These include numerical convergence properties as well as uncertainties associated with the bulge–disc decomposition method and the size of the radial aperture used in the evaluation of equation (2). Here, we present a resolution convergence test of our coupled accretion and feedback model, evaluate the dependence of our results on the hydrodynamics solver employed, and explore the implications of different definitions of host galaxy bulge mass on the simulated $M_{\rm BH}$–$M_\star$ relation.

A1 Resolution convergence

In order to test our results for numerical convergence, we replicate our fiducial simulation with eight times higher mass resolution and two times higher force resolution by evolving 2×512^3 particles down to $z = 2$ in a $[20\,h^{-1}\,{\rm Mpc}]^3$ comoving volume. With the exception of the force softening length, all model parameters are identical to that of our fiducial simulation with 2×256^3 particles, including the number of neighbours used in the black hole accretion and feedback parametrization.

Fig. A1 shows the $M_{\rm BH}$–$M_\star$ relation at $z = 2$ corresponding to our high-resolution simulation. The best power-law fit for galaxies with $M_\star > 10^{9.5}$ M$_\odot$, indicated by the orange solid line, is in good agreement with the local observed $M_{\rm BH}$–$M_{\rm bulge}$ relation of Häring & Rix (2004), though with slightly higher normalization. Indeed, compared to the best-fitting relation for our fiducial simulation at $z = 2$ (blue dashed line), the increased resolution yields a very similar slope but ∼0.25 dex higher normalization. Lower gravitational resolution may result in the underestimation of disc fractions with the consequent reduction in black hole accretion rates relative to higher resolution simulations (Anglés-Alcázar et al. 2015). The numerical resolution tests presented in Anglés-Alcázar et al. (2013) showed very good convergence of the $M_{\rm BH}$–$M_\star$ relation between simulations 5 and 40 times higher mass resolution relative to our fiducial simulation. This suggests that the simulations presented here may have not yet reached full numerical convergence relative to the black hole accretion model. Alternatively, a difference in the normalization of the $M_{\rm BH}$–$M_\star$ relation for simulations with different resolution could partially arise owing to higher efficiency of feedback in simulations with lower resolution (Bourne, Zubovas & Nayakshin 2015). None the less, while the normalization of the $M_{\rm BH}$–$M_\star$ relation is mildly sensitive to resolution, the overall trends described in this work are unchanged. A modest re-normalization of $\epsilon_{\rm T}$ could compensate for the differences in resolution, and our general conclusions are unaffected by this choice.

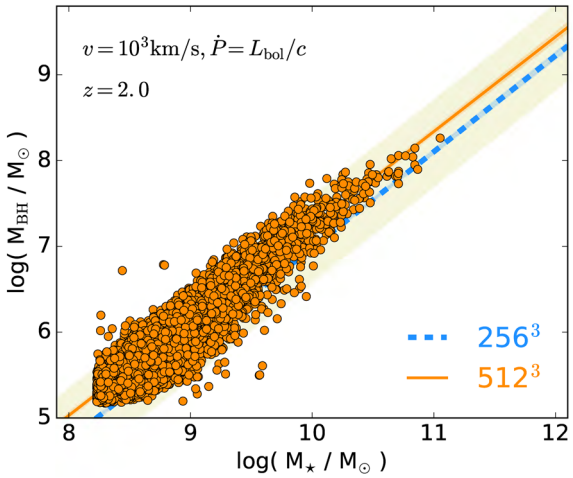

Figure A1. $M_{\rm BH}$–$M_\star$ relation at $z = 2$ obtained for a simulation with eight times higher mass resolution relative to our fiducial simulation, i.e. using 512^3 gas and dark matter particles, but otherwise identical black hole accretion and feedback parameters. The orange solid line indicates the best power-law fit to the $M_{\rm BH}$–$M_\star$ relation for the high-resolution simulation, while the blue dashed line shows the best-fitting relation for our fiducial simulation. The beige shaded area corresponds to 0.5 dex scatter in $M_{\rm BH}$ relative to Häring & Rix (2004). The increased resolution yields a very similar $M_{\rm BH}$–$M_\star$ relation.

A2 Hydrodynamics solver

We take advantage of the multi-method nature of the GIZMO code to evaluate the robustness of our results with respect to the hydrodynamics solver. In particular, we compare our results using a pressure–entropy formulation of SPH with the Lagrangian Godunov-type MFM method implemented in GIZMO (Hopkins 2015). Fig. A2 shows the $M_{\rm BH}$–$M_\star$ relation at $z = 0$ resulting from a simulation using the MFM hydrodynamics solver to evolve 256^3 gas resolution elements in a $[20\,h^{-1}\,{\rm Mpc}]^3$ comoving volume. The initial conditions and model parameters are identical to that of our fiducial simulation. The only exception is the use of a cubic spline kernel with 32 neighbours instead of the quintic spline kernel with 64 neighbours used in our SPH simulations (since MFM converges at lower neighbour number). None the less, to preserve the physical scale at which black hole accretion and feedback are evaluated, the number of neighbours used for the black hole accretion and feedback prescriptions in the MFM simulation is the same as in the SPH simulations (∼256 particles).

The $z = 0$ $M_{\rm BH}$–$M_\star$ relation obtained with MFM is in very good agreement with the observed $M_{\rm BH}$–$M_{\rm bulge}$ relation, with most black hole–galaxy pairs located within 0.5 dex of the Häring & Rix (2004) relation. Compared to our fiducial SPH simulation (Fig. 1), MFM produces slightly larger scatter in the low-mass regime. Considering the best power-law fit to the $M_{\rm BH}$–$M_\star$ relation for galaxies with $M_\star > 10^{9.5}$ M$_\odot$ (indicated by the orange solid line), MFM yields slightly steeper slope and lower normalization relative to our fiducial simulation (blue dashed line). Overall, the good agreement between the two hydrodynamic methods,

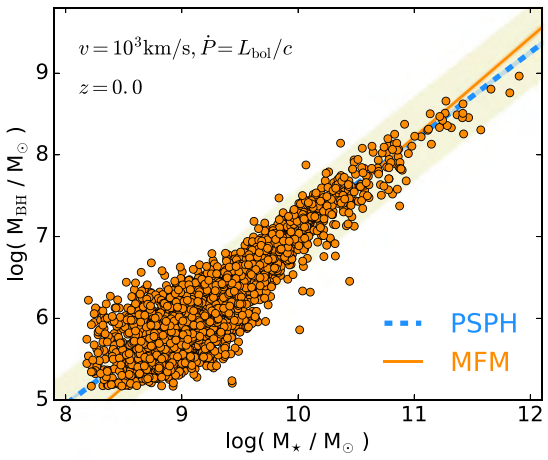

Figure A2. $M_{\rm BH}$–$M_\star$ relation at $z = 0$ obtained for a simulation using the Godunov-type MFM hydrodynamics solver in GIZMO but otherwise identical black hole accretion and feedback parameters as our fiducial simulation (which used P-SPH, the pressure formulation of smoothed particle hydrodynamics). The orange solid line indicates the best power-law fit to the $M_{\rm BH}$–$M_\star$ relation for the MFM simulation, while the blue dashed line shows the best-fitting relation for our fiducial P-SPH simulation. The beige shaded area corresponds to 0.5 dex scatter in $M_{\rm BH}$ relative to Häring & Rix (2004). MFM and P-SPH agree well: our uncertainties are not driven by the hydrodynamic method.

with no additional calibration of model parameters, confirms that our conclusions are not sensitive to the choice of hydrodynamics solver.

A3 Bulge–disc decomposition

Throughout this paper, the stellar mass within the effective radius of the galaxy ($M_\star$) has been used as proxy for bulge mass when comparing simulation results to the observed $M_{\rm BH}$–$M_{\rm bulge}$ relation. This type of simplification is commonly used in cosmological simulations (e.g. DeGraf et al. 2015; Sijacki et al. 2015) and is motivated by the uncertainty in bulge–disc decompositions at the typical resolution achieved in cosmological simulations. Indeed, producing galaxies with realistic bulges continues to be a challenge even for high-resolution cosmological 'zoom-in' simulations (Brooks & Christensen 2016). In contrast, numerical convergence for the stellar mass of galaxies in cosmological simulations is significantly better than any estimate of the bulge component, allowing for a simple but robust quantification of the relative growth of black holes and galaxies. In addition, using $M_\star$ facilitates comparisons with observational studies at higher redshifts, where bulge masses are difficult to estimate (e.g. Jahnke et al. 2009; Sun et al. 2015). Here, we address the robustness of our conclusions to the specific proxy for bulge mass used when comparing our numerical results to the observed $M_{\rm BH}$–$M_{\rm bulge}$ relation.

Fig. A3 shows the $M_{\rm BH}$–$M_\star$ relation at $z = 0$ for our fiducial simulation using two different definitions of host galaxy bulge mass. We perform a simple bulge–disc kinematic decomposition using the full three-dimensional information available in the simulation. For each galaxy, we compute the angular momentum vector of the stellar component, which is used as the reference axis to calculate the azimuthal velocity (v_ϕ) of each star particle. The mass of the spheroidal component ($M_{\rm bulge}$) is estimated as double the mass of particles moving with $v_\phi < 0$ (Abadi et al. 2003). The left-hand panel of Fig. A3 shows the $M_{\rm BH}$–$M_\star$ relation for the total spheroidal component. On average, $M_{\rm bulge}$ is larger than the stellar mass within the effective radius, which yields ∼0.16 dex lower normalization in the best-fitting relation relative to the best power-law fit using our standard definition of $M_\star$. Our simulated galaxies tend to have higher bulge fractions than observed galaxies due to the limited resolution and the lack of star formation-driven winds (Anglés-Alcázar et al. 2014). The right-hand panel shows the $M_{\rm BH}$–$M_\star$ relation for the spheroidal component computed only for star particles within the effective radius of the galaxy, $M_{\rm bulge}(R_{\rm e})$.

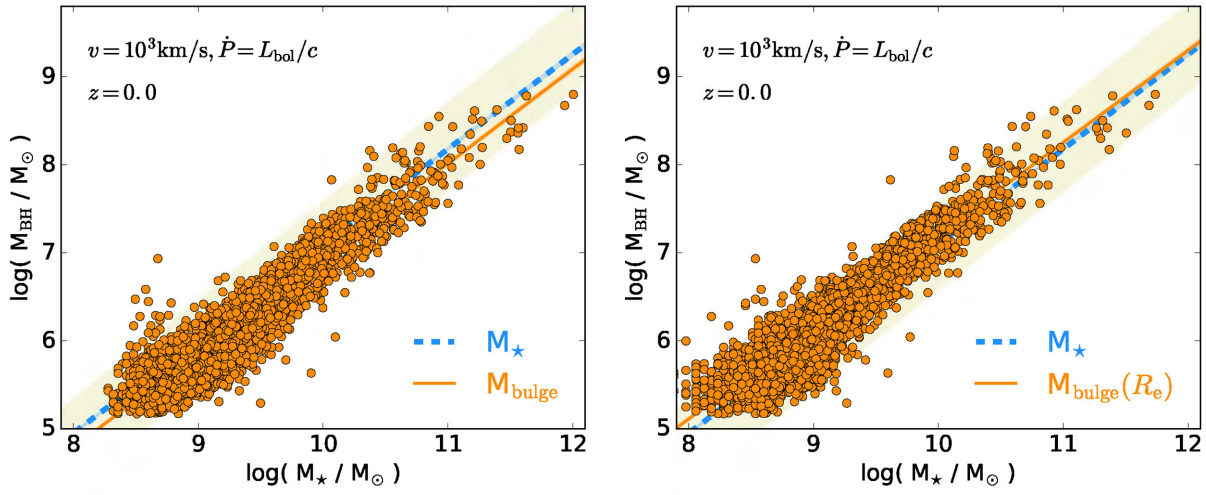

Figure A3. $M_{\rm BH}$–$M_\star$ relation at $z = 0$ for our fiducial simulation using different definitions of host galaxy bulge mass. Left: $M_{\rm BH}$ is plotted against the total mass of the spheroidal component computed using a full three-dimensional kinematic decomposition. Right: same as the left-hand panel for the bulge mass computed within the effective radius of the galaxy. The orange solid lines indicate the best power-law fit to the $M_{\rm BH}$–$M_\star$ relation for the new $M_\star \equiv M_{\rm bulge}$ definitions. The blue dashed lines show the best-fitting relation for our standard definition, where $M_\star$ is computed as the total stellar mass within the effective radius of the galaxy. The beige shaded area corresponds to 0.5 dex scatter in $M_{\rm BH}$ relative to Häring & Rix (2004). Similar scaling relations are obtained regardless of the exact definition of $M_{\rm bulge}$ employed in our large-volume cosmological simulations with relatively limited resolution.

In this case, $M_{\rm bulge}(R_{\rm e}) \leq M_{\star}$ and the best power-law fit yields $\sim$0.10 dex higher normalization and slightly lower slope compared to our standard definition of the $M_{\rm BH}$–$M_{\star}$ relation. Within the limitations of our simulations, our results are thus independent of the proxy for bulge mass. Higher resolution zoom-in simulations (e.g. Hopkins et al. 2014) will be necessary to model galaxies with realistic bulges and properly address whether our black hole model predicts different correlations between $M_{\rm BH}$ and various galaxy components.

This paper has been typeset from a TEX/LATEX file prepared by the author.